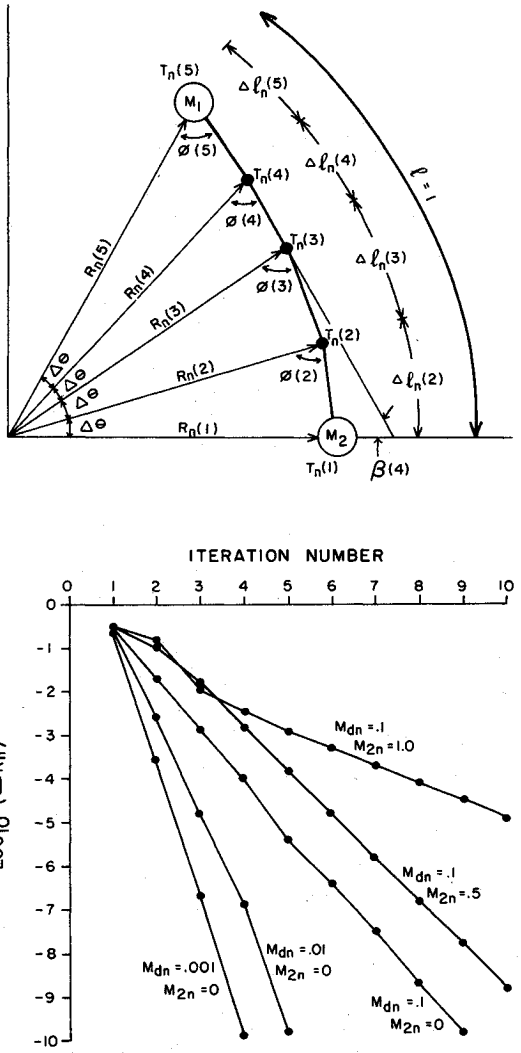

Fig. 2 a) Lumped parameter model used in the algorithm for the case of five lumped masses; and b) plot of the rms difference between iterations against the iteration number for six different combinations of parameter values, showing the rapid convergence of the algorithm.

variable in the computer implementation of the algorithm, and then reducing it as desired.

Observation of Eqs. (6) suggests the following procedure. First, guess a tether "shape" that will determine initial values for R_n, $\Delta\ell_n$, ϕ, and β at each discrete position along the tether. The initial values of R_n are placed in the array $[R_n(K)]_0$, where the subscript 0 designates the zeroth iteration. Then use these values in Eq. (6a) to find the initial array $[T_n(K)]_0$ at each position, sequentially starting at the upper boundary where $T_n(K)_0$ is given by Eq. (7b) and working down from $k = K$ to 1. Next, use all of the zeroth iteration values in Eq. (6b) to find a new angle β at each discrete position by starting at the $k = 1$ boundary value given by Eq. (7a) and working up through $k = K$. The updated "shape" is embodied in this $[\beta(K)]_1$ array, which gives a new curvature at each point. It can be used to update the R_n, $\Delta\ell_n$, ϕ, and β arrays using only geometrical considerations and the total length condition (7c). The updated $[R_n(K)]$ array then can be used to start a new iteration.

This procedure can be repeated indefinitely giving a series of values for $[R_n(K)]_m$, which, it is hoped, will converge as m increases. If it does converge, the result must satisfy Eqs. (6) and (7) and, therefore, must be a solution to the problem. A mathematical proof of convergence is not attempted here, but a computer program implementing the preceding scheme has been observed to converge for all reasonable parameter values and for two very different starting tether shapes. The convergence was measured by taking the rms difference ΔR_n between successive values of the $[R_n(K)]_m$ array, the results of which are shown in Fig. 2b for six combinations of system parameters. Note that the rate of convergence is faster for lower values of the tether mass density and for lower values of the mass M_2.

Now that the statics problem has been solved, it is being used as the starting point in the calculation of the dynamic response of the same system when gravity gradients, solar radiation pressure, atmospheric drag, and thermal expansion forces are present. In turn, this will be used to model a system designed to control the attitudes and positions of the collimating telescopes in the proposed interferometer.

References

[1]Vakili, F., "Triangle: A Different Design for a Three Satellite Interferometer in Space," *ESA, Proceedings of the Colloquium on Kilometric Optical Arrays in Space,* European Space Agency, Noordwijk, The Netherlands, SP-226, April 1985, p. 107.

[2]Crellin, E. B., "Preliminary Studies of a Spinning Tether-Connected Trio Concept," *ESA, Proceedings of the Colloquium on Kilometric Optical Arrays in Space,* European Space Agency, SP-226, April 1985, p. 91.

[3]Goodman, J. W., "Statistical Optics," Wiley, 1985, pp. 207–211.

Generation of Infrared Earth Radiance for Attitude Determination

T. K. Alex* and Ramani Seshamani†
ISRO Satellite Centre, Bangalore, India

Introduction

INFRARED Earth sensors, which detect the infrared horizon of the Earth in the 15 μm carbon dioxide band, determine the roll and pitch errors of the spacecraft.[1] The Earth chord width and the reference time signals synchronized with the scanning are used to derive the attitude errors. Generally, these sensors detect the relative change in the radiation at the horizon by differentiating the preamplified electronic signal from the detector. Since there is a radiance gradient across the Earth, the differentiator output from the Earth sensor will tend to give a constant offset, the sign and the amplitude of which depend upon the direction of the gradient and the slope of the gradient, respectively, the slope being inversely proportional to the angular width of the Earth as seen from the satellite. Whereas for a low-Earth orbiting satellite the offset error is $\approx$0.6 deg, for a geostationary satellite it is $\approx$0.15 deg. Whereas for earlier spacecraft, which had more symmetric configurations and less stringent payload

Received Nov. 5, 1987.

*Head, Sensor Systems Division.
†Engineer, Sensor Systems Division.

pointing accuracy requirements, the attitude determination tasks could be done on ground using daily monitoring of telemetered attitude sensor data, the recent generation of spacecraft, such as Intelsat VI, require precise antenna beam pointing to within 0.04 deg of the orbit normal, which needs attitude corrections two to five times per day, due to the high attitude precession rates. This has necessitated the development of onboard spin axis controllers.[2] The other high-precision attitude determination requirements occur during the apogee motor firing in geostationary transfer orbit and for remote sensing Earth-pointing payloads in low-Earth orbit.

Some studies have been carried out to model the radiance profile in terms of tangent height,[3] latitude, and month.[4] However, analytical models are not valid when horizontal temperature gradients are present in the middle atmosphere,[1] which is representative of the actual situation. The model presented in this Note is a generalized model, giving the radiance as a function of the geographical location and the time of the year.

Data and Analysis

With the aim of developing a model of the Earth's infrared radiance in the 15 μm carbon dioxide band, radiance data were collected and analyzed. The radiance values in Wm^{-2} sr^{-1} were taken from the observational data of the ESRO-IV horizon crossing indicator.[5] Radiance data over a range of latitudes from 80°N 80°S during the period December 1972–April 1974 were taken for the analysis. Radiance data from the Indian satellite BHASKARA-I observations with its two horizon sensors were also taken[6] during the period July–November 1979. The longer-term variations in radiance were modeled by considering data over the period 1964–1979 from several data sources.[7-9]

Since latitude, time of the year, and the year are the three independent variables on which the radiance is dependent (the model was averaged over longitude, since the longitude-dependent effects are negligible), the radiance is expressed in terms of X (latitude), Y (time of the year $=0.0$ on Jan. 1, $=12.0$ on Dec. 31), and Z (year) as follows:

$$F_1(Y) = \cos(\pi Y)/6$$

$$F_2(Y) = 1 - \frac{Y}{3} \text{ for } Y < 6$$

$$= \frac{Y}{3} - 3 \text{ for } Y > 6$$

$$X_m = 2.5 + 10F_1(Y)$$

Z = year

Z_{min} = year of the minimum of the solar sunspot cycle: 1986.5, 1997.5 ....

Z_{max} = year of the maximum of the solar sunspot cycle: 1979.5, 1990.5 ....

We have the following equations for the radiance F. For $X < X_m$

$$F = 5.0 + 2.6\left[\sin^2\left(\frac{\pi(X - X_m + 12.5)}{2(90 + X_m - 12.5)}\right) - \sin^2\left(\frac{12.5\,\pi}{2(90 + X_m - 12.5)}\right)\right]F_1(Y) + 0.3(Z - Z_{min}) - 0.425$$

for $Z > Z_{min}$ (1a)

or

$$-0.17(Z - Z_{max}) + 0.775 \text{ for } Z < Z_{min} \quad (1b)$$

For $X > X_m$

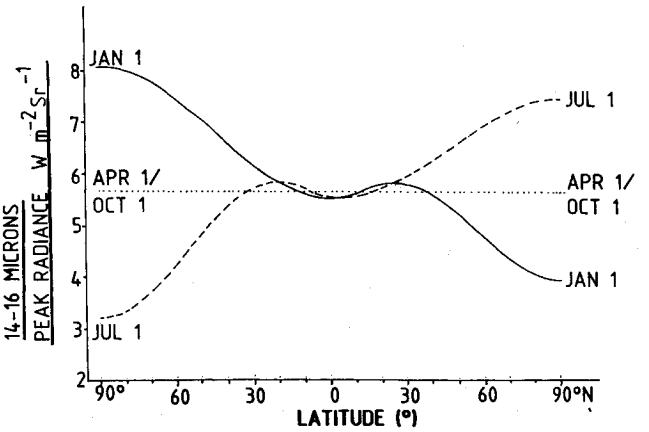

Fig. 1 Radiance values in January, April, July, and October 1990.

Table 1 Radiance values for 1988, from 90°S to 90°N, $Wm^{-2}sr^{-1}$

Lat.	Jan.1	Feb. 1	March 1	April 1	May 1	June 1	July 1	Aug. 1	Sept. 1	Oct. 1	Nov. 1	Dec. 1
−90	7.503	7.154	6.318	5.067	3.860	2.953	2.625	2.933	3.824	5.025	6.281	7.175
−80	7.425	7.084	6.272	5.066	3.914	3.060	2.753	3.041	3.880	5.025	6.237	7.105
−70	7.199	6.884	6.141	5.061	4.066	3.359	3.114	3.344	4.037	5.025	6.109	6.903
−60	6.853	6.578	5.942	5.053	4.289	3.794	3.635	3.784	4.268	5.025	5.915	6.595
−50	6.429	6.205	5.702	5.045	4.547	4.282	4.214	4.277	4.534	5.025	5.681	6.219
−40	5.977	5.811	5.453	5.036	4.793	4.730	4.735	4.730	4.789	5.025	5.439	5.821
−30	5.553	5.444	5.228	5.029	4.987	5.052	5.095	5.055	4.988	5.025	5.220	5.451
−20	5.207	5.152	5.059	5.024	5.093	5.188	5.224	5.190	5.097	5.025	5.056	5.155
−10	4.982	4.969	4.967	5.022	5.096	5.111	5.096	5.110	5.097	5.025	4.967	4.969
0	4.903	4.918	4.964	5.024	5.013	4.975	4.943	4.974	5.012	5.025	4.966	4.917
10	4.982	5.007	5.042	5.026	4.989	4.963	4.942	4.962	4.988	5.025	5.042	5.006
20	5.166	5.122	5.077	5.026	5.011	5.037	5.067	5.038	5.012	5.025	5.075	5.124
30	5.166	5.103	5.045	5.024	5.076	5.188	5.300	5.192	5.079	5.025	5.043	5.105
40	4.954	4.952	4.953	5.021	5.175	5.394	5.609	5.401	5.181	5.025	4.954	4.953
50	4.580	4.703	4.819	5.017	5.291	5.626	5.953	5.637	5.301	5.025	4.824	4.700
60	4.129	4.411	4.670	5.013	5.407	5.852	6.285	5.867	5.421	5.025	4.680	4.402
70	3.704	4.139	4.535	5.009	5.505	6.041	6.560	6.059	5.523	5.025	4.550	4.125
80	3.402	3.947	4.442	5.006	5.571	6.166	6.742	6.185	5.590	5.025	4.460	3.930
90	3.293	3.879	4.408	5.006	5.595	6.210	6.806	6.230	5.614	5.025	4.427	3.860

$$F = 5.0 - 1.9\left[\sin^2\left(\frac{\pi(X - X_m - 12.5)}{2(90 - X_m - 12.5)}\right) - \sin^2\left(\frac{12.5\,\pi}{2(90 - X_m - 12.5)}\right)\right]F_2(Y) + 0.3(Z - Z_{\min}) - 0.425 \quad \text{for } Z > Z_{\min} \quad (2a)$$

or

$$-0.17(Z - Z_{\max}) + 0.775 \quad \text{for } Z < Z_{\min} \quad (2b)$$

where F = radiance in the 15 μm band measured by the spacecraft Earth sensor, expressed in $\mathrm{Wm^{-2}\ sr^{-1}}$.

Figure 1 shows the radiance model for January 1, April 1, July 1, and October 1 for the year 1990. These plots are typical. Radiance values generated by the model for the year 1988 are listed in Table 1. In case of onboard correction, the data can be stored in table lookup form. Alternatively, since the radiance model is in algebraic form, which can be computed using microprocessors, it enables onboard correction of the systematic errors of the horizon sensor. This will need, additionally, the use of the onboard timer, orbit generator programs, and mathematical routines for locating the coordinates of the horizon. Deviations from the longitudinally averaged radiance caused by mesoscale weather patterns, sudden polar stratospheric warmings, etc., are not accounted for in the model.

Conclusion

This Note has proposed a radiance model for use in planning, simulating, and testing Earth sensor-based attitude determination software for postfacto orbit refinement, and also for the implementation of attitude determination and control schemes onboard spacecraft. An equation is developed for the latitudinal, daily, and yearly variation of radiance. Using this equation either in table lookup form or by numeric processing onboard, correction for the radiance gradient effect can be incorporated by suitable transformation of the radiance gradient to roll and pitch errors.

References

[1]Wertz, J. R. (ed.), *Spacecraft Attitude Determination and Control,* D. Reidel, Boston, MA, 1978.

[2]Chen, C. L., Slafer, L. I., and Hummel, W. F., Jr., "Onboard Spin Axis Controller for a Geostationary Spin-Stabilized Satellite," *Journal of Guidance, Control, and Dynamics,* Vol. 10, May-June 1987, pp. 283-290.

[3]Thomas, J. R., Jones, E. E., Carpenter, R. O., and Ohring, G., "The Analysis of 15 Micron Infrared Horizon Radiance Profile Variations Over a Range of Meteorological, Geographical and Seasonal Conditions," NASA CR-725, 1967.

[4]Ward, K. E., "Modelling of the Atmosphere for Analysis of Horizon Sensor Performance," *Sensor Design using Computer Tools,* Vol. 327, Society of Photo-optical Instrumentation Engineers, Bellingham, WA, 1982, pp. 67-78.

[5]Brewer, M. H. and Jones, T. H. P., "Modelling of the Earth Radiance from ESRO-IV HCI Data-Final Report," British Aircraft Corp., Bristol, UK, Rept. ESS/SS 722, 1976.

[6]Seshamani, R., Alex, T. K., Jain, Y. K. Kanakaraju, K., "Solar-Cyclic Variation in Radiation from Atmospheric Carbon Dioxide," *Planetary and Space Science,* Vol. 36, 1988.

[7]Barnes, M. B., Craig, S., and Haskell, A., "The Miranda (X-4) Infrared Experiment: Design, Performance and Earth Radiance Measurements," *Journal of the British Interplanetary Society,* Vol. 33, 1980, pp. 52-65.

[8]McKee, T. B., Whitman, R. I., and Davis, R. E., "Infrared Horizon Profiles for Summer Conditions from Project Scanner," NASA TN-D-4741, 1968.

[9]Peterson, R. E., Schuetz, J., Shenk, W. E., and Tang, W., "Derivation of a Meteorological Body of Data Covering the Northern Hemisphere in the Longitude Region Between 60°W and 160°W from March 1964 through February 1965," NASA CR-723, 1967.

On the Method of Matched Asymptotic Expansions

D. S. Naidu*
Old Dominion University, Norfolk, Virginia
and
D. B. Price†
NASA Langley Research Center, Hampton, Virginia

Introduction

SINGULAR perturbation problems, where suppression of a small parameter affects the order of the problems, have been solved by a wide variety of techniques.[1-5] Two of these techniques, the singular perturbation method (SPM)[1,5] and the method of matched asymptotic expansions (MAE),[2,3] have been developed independently to a reasonable level of satisfaction. Essentially, SPM consists of expressing the total solution in terms of an *outer* solution, an *inner* solution, and an *intermediate* solution. On the other hand, in the method of MAE, a composite solution is constructed as the outer solution, the inner solution, and a *common* solution.

In this Note, a critical examination of the MAE method reveals that the various terms of the common solution of MAE can be generated as polynomials in stretched variables without actually solving for them from the outer solution as is done presently. This also shows that the common solution of the MAE method and the intermediate solution of SPM are the same and, hence, that these methods give identical results for a certain class of problems. An illustrative example is given.

Method of Matched Asymptotic Expansions

The method of matched asymptotic expansions has been used extensively in fluid mechanics.[2] In this method, a composite solution is expressed as an outer solution, plus an inner solution, and minus a common solution

We describe briefly the MAE method as applicable to initial-value problems. Consider

$$\frac{dx}{dt} = f(x,z,\epsilon,t) \quad (1a)$$

$$\epsilon\frac{dx}{dt} = g(x,z,\epsilon,t) \quad (1b)$$

where x and z are n- and m-dimensional state vectors, respectively, and ϵ a small positive parameter responsible for singular perturbation. We begin by representing the solutions in the form of a series in powers of ϵ as

$$x(t,\epsilon) = \sum_{i=0}^{\infty} x^{(i)}(t)\,\epsilon^i \quad (2a)$$

$$z(t,\epsilon) = \sum_{i=0}^{\infty} z^{(i)}(t)\,\epsilon^i \quad (2b)$$

and determine the various terms $x^{(i)}(t)$ and $z^{(i)}(t)$ by means of formal substitution of Eqs. (2) in Eqs. (1) and comparison of coefficients of equal powers of ϵ. Then the following set of

Received Oct. 13, 1987; revision received Dec. 18, 1987.

*Associate Research Professor, Department of Electrical and Computer Engineering. Member AIAA.

†Assistant Head, Spacecraft Control Branch. Member AIAA.